PAPER

Associative *vs.* dissociative binding of CO_2 on M_4 transition metal clusters

Sherfi Sherif, Bala Aakash Velmurugan, Naeem Abbas, Muskanbanu Shaikh and Matthew A. Addicoat [ID] *

Density functional theory calculations were performed to determine reaction paths for the reaction of CO_2 with M_4 transition metal clusters (M = Nb, Mo, Ru, Rh, Pd, Ag, Pt). Geometries incorporating associatively bound (CO_2), partly dissociated (O + CO) and fully dissociated (O + C + O) carbon dioxide were identified for all clusters except Ag_4. Nb_4 and Mo_4 are likely to dissociate CO_2 fully. For Ru_4, both partly and fully dissociative geometries were competitive, while Rh_4, Pd_4 and Pt_4 activate CO_2 without breaking either CO bond. Ag_4 was found to interact only minimally with CO_2. The change in ν_{bend}, the energy of the CO_2 π_u orbital in the physisorbed M_4CO_2 capture species and the charge transfer to the CO_2 molecule, $q(CO_2)$, in the first transition state were found to correlate with the eventual fate of the CO_2 molecule.

1 Introduction

Carbon dioxide CO_2, is one of the key pollutant gasses contributing to global warming and ocean acidification.[1] In recognition of the urgency of this problem, in recent years there have been increasing efforts to develop and deploy carbon capture and storage systems. To go one step further, rather than storing carbon captured from the atmosphere (as CO_2), valorizing it as a C_1 feedstock. Captured CO_2 could be used to produce common feedstock chemicals and fuels such as formaldehyde, methanol and formic acid.[2,3] Reduction of CO_2 *via* the reverse Water Gas Shift (rWGS) reaction produces carbon monoxide, CO, that can be employed in a variety of industrially relevant reactions.[4,5]

Somewhat frustrating the aim of employing captured CO_2 as a reactant in various chemical processes, is its exceptional thermodynamic and kinetic stability: the Gibbs free energy of formation, $\Delta_f G$ at 298 K is -394.36 kJ mol^{-1}.[6] Therefore, activating the CO_2 molecule, by partly or fully breaking one of the two C=O bonds requires one or more of; a careful choice of reactants that can donate to the CO_2 molecule, a similarly careful choice of product, shifting the equilibrium – *e.g.* by removing product, and a large energy input.[7]

Considering the mechanism of how a catalytic system can activate CO_2, upon CO_2 adsorption or coordination to the system, often at the site of a metal centre, electron density is introduced into the antibonding π^* orbitals of CO_2. The C=O bonds are thereby weakened and the molecule subsequently

adopts a bent geometry ($\theta_{OCO} \approx 120–140°$), creating a dipole and increasing the reactivity of CO_2.[7–11]

A variety of novel catalysts for the activation of CO_2 have been proposed, including MOFs,[12–14] ceria[15,16] and a variety of metal (oxide) surfaces including Fe,[17] Ti,[18] Cu[19] and Pd/Mo.[20] A key feature of all of these proposed catalysts is that they involve one or more metal atoms at the active site as the source of the electron density donated to the CO_2 molecule.

Transition metal clusters have been studied both experimentally and computationally for many years for their capacity to adsorb and activate various small molecules including CO_2.[21,22] Transition metal clusters were initially studied as models of bulk surfaces.[23] However, it was rapidly identified that the properties of these clusters is both size-[24] and geometry-dependent,[25,26] and therefore, that by modifying the size and composition of the (nano)clusters, that the properties, especially the reactivity, of the clusters could be tuned.[23,27,28] Most recently, transition metal clusters have been confined within the pockets of porous framework materials, with the goal of protecting the active metal clusters from sintering, whilst the porous framework still allows mass transfer.[29,30]

Computational studies, normally employing density functional theory (DFT), are key in determining the geometric structures and reaction mechanisms in both gas-phase[31–33] and surface studies,[34] especially identifying where barriers may prevent thermodynamic products from being observed.[35] A recent DFT-based mechanistic study from Mondal *et al.* showed that beyond simply the static cluster geometry, the fluxionality of the cluster was important in determining the reduction of CO_2 on supported copper tetramers.[36] Da Silva and coworkers studied a the reverse water gas shift reaction on

School of Science and Technology, Nottingham Trent University, Clifton Lane, Nottingham, NG11 8NS, UK. E-mail: matthew.addicoat@ntu.ac.uk

series of M_{13} clusters, M = Fe–Cu and observed that increasing the d-state occupation favoured COOH formation.[5] Recently, Mohanta and Jena attempted to address the poor selectivity of the Cu_{13} cluster by investigating a series of XCu_{12} clusters, where X was a variety of first and second row transition metal atoms.

With a similar aim of understanding cluster behaviour across the periodic table, in this work, we present DFT calculated reaction paths for CO_2 addition to second row M_4 transition metal clusters from Nb_4 to Ag_4, we exclude technetium, due to its radioactivity, but we include the third-row Pt_4 cluster due to the popularity of platinum as a catalyst.

2 Computational method

Structures of M_4 clusters, for M = Nb–Ag (excluding Tc) and Pt were generated using the Kick stochastic structure search procedure with four individual M atoms supplied.[37,38] Full searches were undertaken on the lowest possible multiplicity (singlet for all M_4 clusters) and all minima identified were re-optimized at higher multiplicities. For all species, the lowest four multiplicities were calculated, but for rhodium, palladium and platinum, the search was extended up to the nonet. Ruthenium is known to have low lying minima with high numbers of unpaired electrons and so the search was further extended up to the 15-tet. No symmetry was imposed at any point in the search, nevertheless, several clusters adopted clear point group symmetry, as evidenced by geometric parameters and frequencies. Where point group symmetry was observed in either bare M_4 or M_4CO_2 clusters, we refer to this apparent symmetry, but we did not confirm the symmetry by further constrained calculation, as the addition of CO_2, or further steps on the reaction path would immediately break symmetry.

The lowest energy structure of each M_4 cluster was then adopted as a fragment in a further stochastic search process. Kick runs were undertaken searching for with the following configurations: $M_4 + CO_2$ (*i.e.* intact CO_2); $M_4 + CO + O$; $M_4 + C + O + O$. As activation of the CO_2 molecule is expected to proceed *via* electron donation into the CO_2 π_u orbitals, thus bending the CO_2 molecule,[10] two Kick runs were also undertaken explicitly searching for minima and transition states, employing the M_4 cluster and a bent CO_2 molecule as fragments. Additional starting geometries were generated by hand (*e.g.* CO_2 bound to different symmetry-distinct metal atoms, end-on/side-on, linear/bent, $\mu^1/\mu^2/\mu^3$-bound). From these calculations, the physisorbed "capture" species and the M_4CO_2 global minimum were identified, and the reaction pathway was then filled in and confirmed by a series of Quasi-Synchronous Transit (QST) and Intrinsic Reaction Coordinate (IRC) calculations. Where the global minimum was not a dissociated structure (*i.e.* $M_4 + O + C + O$), the lowest energy dissociated structure was also identified and a pathway to that structure was calculated using QST and IRC calculations as above.

The zero energy for each $M_4 + CO_2$ system is defined as the sum of the energies of the M_4 metal cluster in the singlet multiplicity and the CO_2 molecule. Thus structures with a negative relative energy (below zero energy) are more stable than the separated reactants; structures with a positive relative energy (energy higher than zero energy) are unstable with respect to the infinitely separated reactants. As in a previous study, basis set superposition error (BSSE) was disregarded, as were zero-point energies and entropic contributions.[39] All structure searches (Kick runs) were undertaken with the B3P86 density functional[40] and Stuttgart Relativistic Small Core (SRSC) basis set,[41–43] as previous studies[39,44] have shown this to be an accurate and computationally efficient combination. The final pathways were re-optimized at all relevant multiplicities using the TPSS functional[45] with the Def2TZVP basis set[46,47] and employing the D3-BJ empirical dispersion term.[48] This latter combination, while more expensive, has also been shown to reproduce energetic ordering and vibrational data for reactions of small molecules on gas phase transition metal clusters including Rh_n[49] and Pt_n.[50] Gaussian 16 was used for all calculations.[51] Absolute and relative energies for all structures calculated with both functionals are presented in the SI (xlsx), structures are included in xyz format (zipfile).

3 Results and discussion

All M_4 tetramers are even-electron species, and thus we calculate the singlet – septet surfaces by default.

3.1 Nb_4

For the Nb_4 cluster we find a tetrahedral structure of singlet multiplicity to be the lowest in energy, in line with previous calculations using several DFT methods,[52–55] and confirmed by coupled cluster[56] and multireference singles and doubles configuration interaction (MRSDCI).[57] This cluster was used for the CO_2 pathway without constraint.

The $Nb_4 + CO_2$ pathway is shown in Fig. 1 and the corresponding geometric data is tabulated in Table S1. Only the singlet and triplet surfaces are shown as the quintet and septet were high in energy. The capture species (Fig. 1-I) is bound by −0.29 eV and consists of the CO_2 molecule approaching one vertex of the Nb_4 tetrahedron. The CO_2 molecule bends in the first transition state and the central carbon atom is μ^2 bound to a Nb–Nb edge, rotation of the CO_2 molecule over a Nb_3 face allows the first oxygen atom to dissociate (Fig. 1-V) and the remaining CO molecule dissociates the same way over the adjacent face resulting in a fully dissociated global minimum with a relative energy −6.61 eV below zero energy.

3.2 Mo_4

Several groups have undertaken calculations on the Mo_4 cluster: a recent DFT study by Kantorovich and coworkers predicted seven isomers within 1 eV of the global minimum, and two of those structures were separated by only 0.034 eV per atom – both structures were "tetrahedron-like" and possessed D_{2d} symmetry, but differed in the hinge angle.[58] Liebing *et al.* predict a stretched tetrahedral structure,[59] while Yin *et al.*
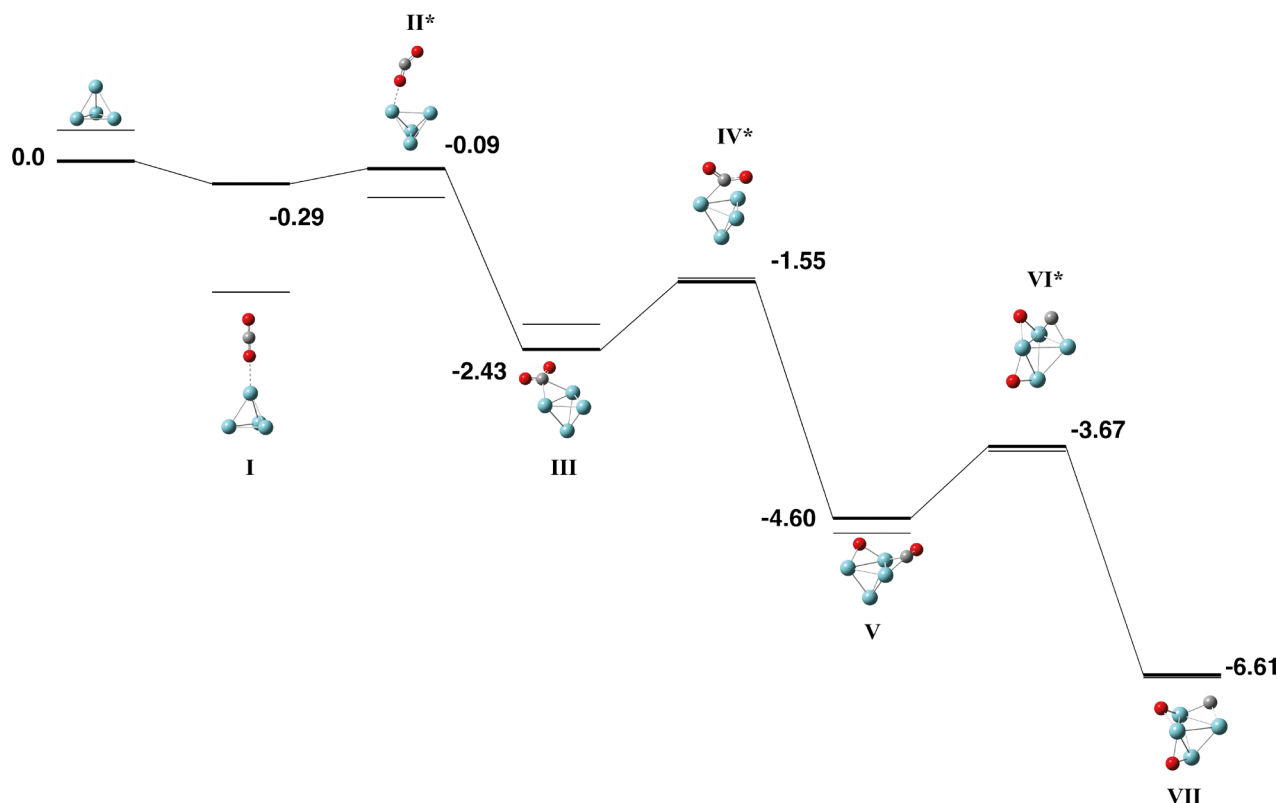
Fig. 1 Stationary points on the $Nb_4 + CO_2$ potential energy surface. The singlet multiplicity is shown in bold and the triplet multiplicity is shown with thin lines. Relative energies are given in eV. Metal atoms are shown in blue/green, oxygen atoms are shown in red and the carbon atom is shown in grey.

predict a tetrahedral global minimum with an open "butterfly" structure 0.34 eV higher in energy.[60] Sumer and Jellinek reverse this order, predicting an open butterfly structure with $\mu_B = 4$ being 0.01 eV per atom lower in energy than a tetrahedral structure with $\mu_B = 2$.[61] Pis Diez undertook a detailed study of the symmetry of the Mo_4 structure and identified four distorted tetrahedra of D_{2d} symmetry, a D_2 structure and a C_{3v} triangular pyramid.[62] Our structure search on the singlet surface identified the open butterfly ($\phi = 130°$), stretched tetrahedron ($\phi = 50°$) and

tetrahedral structures and the open butterfly was employed as a fragment in the reaction path with CO_2. It is to be noted, that despite starting from the open butterfly structure, upon interaction with CO_2, the Mo_4 cluster became more compact, resembling either the tetrahedron or stretched tetrahedral structures.

The reaction path for $Mo_4 + CO_2$ is very similar to that of Nb_4 and is shown in Fig. 2 with the corresponding geometric data in Table S2. The singlet–quintet surfaces are shown as the septet surface is high in energy. The CO_2 molecule initially
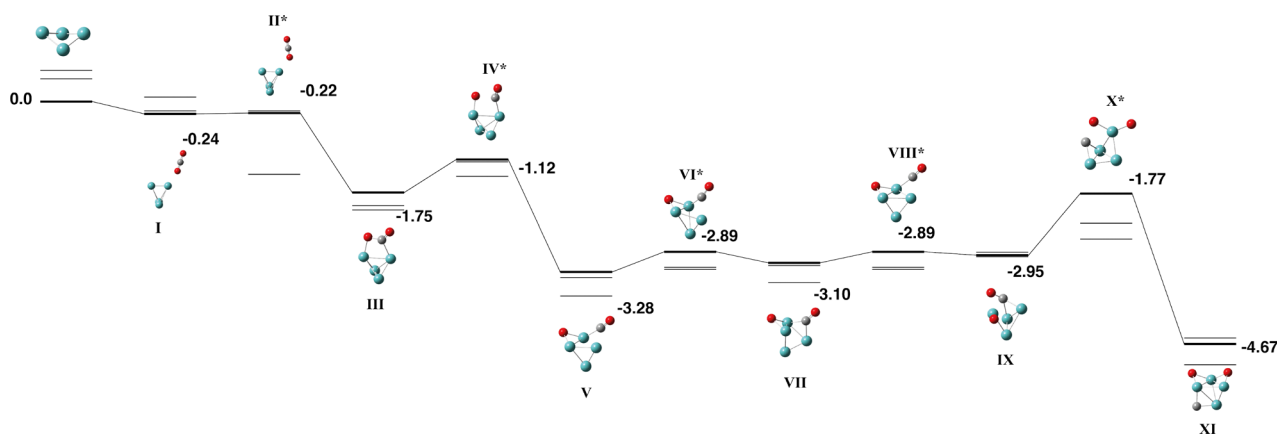

Fig. 2 Stationary points on the $Mo_4 + CO_2$ potential energy surface. The singlet multiplicity is shown in bold and the triplet–quintet multiplicities are shown with thin lines. Relative energies are given in eV. Metal atoms are shown in blue/green, oxygen atoms are shown in red and the carbon atom is shown in grey.

Fig. 3 Stationary points on the $Ru_4 + CO_2$ potential energy surface. The singlet multiplicity is shown in bold and the triplet-13-tet multiplicities are shown with thin lines. Relative energies are given in eV. Metal atoms are shown in blue/green, oxygen atoms are shown in red and the carbon atom is shown in grey.
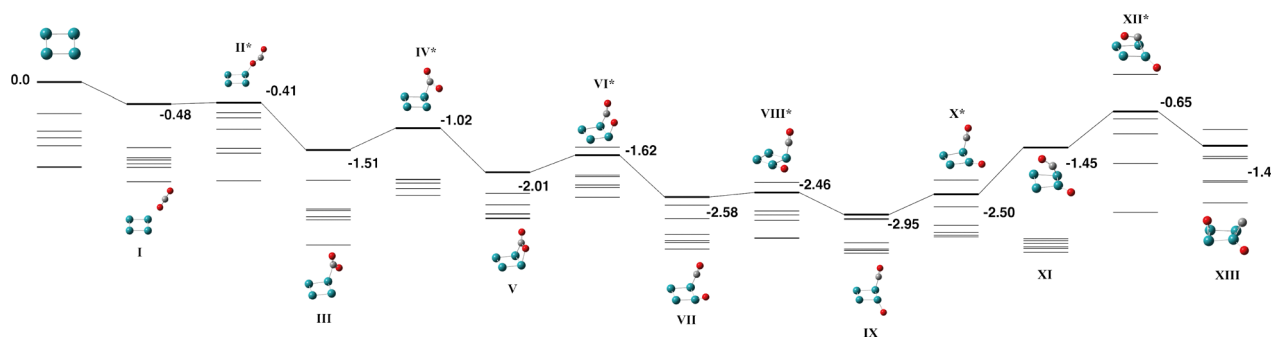
approaches a single Mo atom in the capture species before binding in a η^2 fashion across a Mo–Mo bond (Fig. 2-III). The first O–CO bond breaks to yield a μ^2-bound oxygen atom and a μ^1-bound CO molecule (Fig. 2-V), which rotates to become μ^2-bound (Fig. 2-VII) before dissociating. The lowest energy structure has CO_2 fully dissociated and is −4.67 eV below the energy of the separated Mo_4 (singlet) and CO_2. The equivalent triplet structure is −5.07 eV below zero energy.

3.3 Ru_4

As ruthenium is known to have low-lying states with a high number of unpaired electrons, multipliticities up to 15-tet are investigated for the $Ru_4 + CO_2$ reaction. The lowest energy Ru_4 structure was determined to be a singlet rectangle with side lengths of 2.21 and 2.24 Å which is in approximate agreement with previous calculations on the Ru_4 cluster that predict a D_{4h} singlet square structure.[63–65]

Fig. 3 and Table S3 show the reaction path for $Ru_4 + CO_2$. Multiplicities up to the 13-tet are shown, the 15-tet was approximately 1 eV higher in energy throughout the entire pathway. The CO_2 molecule interacts first with a single ruthenium atom in the capture species (Fig. 3-I), before bending and

rotating to form a Ru–C covalent bond (Fig. 3-III). On the singlet surface this step requires surmounting a barrier at +0.57 eV, but for all other multiplicities, this transition state is below zero energy. The CO_2 molecule rotates to locate one oxygen atom over the adjacent Ru atom, forming a $\mu^2\eta^2$ structure. The lowest energy structure is Fig. 3-IX, where the CO_2 molecule has partly dissociated to a μ^1-bound oxygen atom in the Ru_4 plane and a μ^1-bound CO molecule approximately perpendicular to the plane. The remaining CO molecule can then fall across the Ru_4 face and dissociate (Fig. 3-XIII), however, the dissociation of the second CO bond, while still below zero energy, is less favoured than the partly dissociated CO_2 structure (Fig. 3-VII).

3.4 Rh_4

As with ruthenium, we consider additional multiplicities for the Rh_4 cluster reaction, from singlet–nonet. The lowest energy Rh_4 cluster was identified to be a singlet tetrahedron of T_d symmetry and a side length of 2.45 Å. This result is consistent with that of many authors[66–70] and we employ this structure, without constraint, as a fragment for reaction with CO_2.

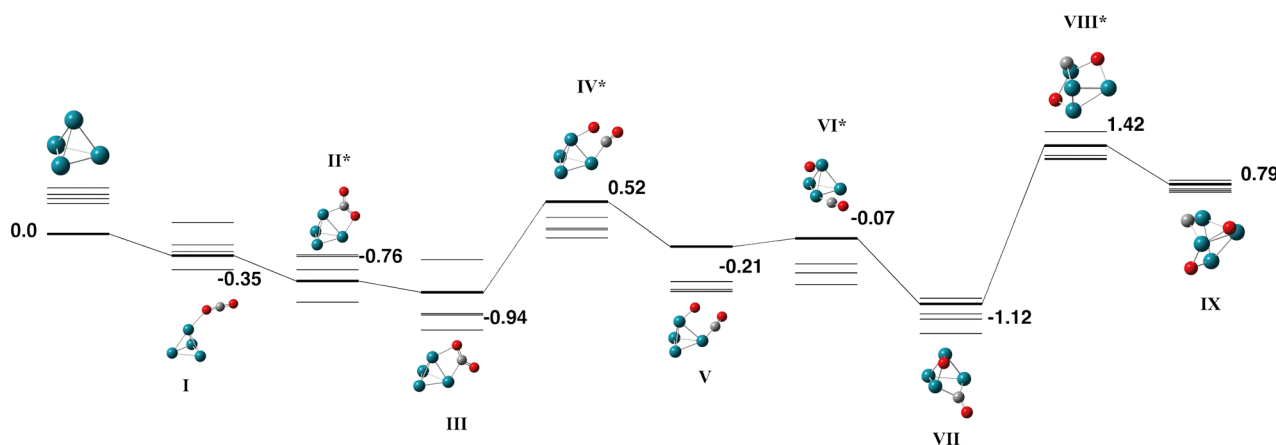Fig. 4 shows the reaction path for $Rh_4 + CO_2$, the corresponding geometric data is tabulated in Table S4. From the

Fig. 4 Stationary points on the $Rh_4 + CO_2$ potential energy surface. The singlet multiplicity is shown in bold and the triplet–nonet multiplicities are shown with thin lines. Relative energies are given in eV. Metal atoms are shown in blue/green, oxygen atoms are shown in red and the carbon atom is shown in grey.

η^1-O bound capture species, the CO_2 molecule falls across a Rh–Rh bond, binding in a $\mu^2\eta^2$ fashion, with a O–C–O angle, $\theta_{OCO} = 140°$, but only marginally lengthening the CO bond ($r_{CO} = 1.26$ and 1.27 Å). The transition state stretching the coordinated CO bond ($\nu_{imag} = 464$ cm^{-1}) is +0.52 eV higher than zero energy. After the first CO bond breaks, both the intact CO molecule and the dissociated oxygen atom rotate around the cluster, shifting from μ^1 to μ^2 binding in the lowest energy Rh$_4$CO$_2$ cluster (Fig. 4-VII). To reach the lowest energy fully dissociated structure, Fig. 4-IX, +0.79 eV above zero energy, the second CO bond needs to be stretched over an adjacent Rh$_3$ face, surmounting a transition state of +1.42 eV. Given that all transition states involving stretching of a CO bond have energy above that of the separated reactants, it is likely that CO_2 would remain intact on the Rh$_4$ cluster.

3.5 Pd$_4$

Pd$_4$ has also been extensively calculated. Futschek *et al.* calculated square, rhombus and tetrahedral structures with different multiplicities and point group symmetries, concluding that the triplet tetrahedron was the global minimum.[67] This assignment is in agreement with Kawazoe and coworkers[71] Moc *et al.* also employ a tetrahedral triplet ($^3A''$) Pd$_4$ structure in their reaction with H$_2$ molecules. Our structure search also identified a triplet global minimum, with a tetrahedral structure, though with a slightly expanded dihedral angle of 74° (*viz.* 80° in the singlet and 70.5° in T_d symmetry). We use this fragment going forward.

In addition to calculations determining the structure of the Pd$_4$ cluster, there have been many DFT studies on reactions of Pd$_4$. Borbolla *et al.* in their B3LYP/6-31G(d,p) study, determined that the adsorption of formic acid on Pd$_4$ would favourably produce CO_2.[72] Lian and coworkers showed that Pd$_4^-$ had a lower barrier to dissociating N$_2$O than the neutral or cationic tetramers[73] and Dutta *et al.* compared the bare and ZSM-5-supported Pd$_4$ cluster for the same reaction.[74] Kalita and Deka calculated reaction profiles for CO oxidation on bare and oxidized Pd$_4$ clusters.[75]

The reaction path calculated for Pd$_4$ + CO$_2$ is shown in Fig. 5 with geometric data in Table S5. The lowest energy species for Pd$_4$CO$_2$ is Fig. 5-III, just after the capture species (Fig. 5-I). In structure Fig. 5-III, the CO$_2$ molecule is bent over a Pd–Pd bond, with $\theta_{OCO} = 136°$ and $r_{CO} = 1.24$ and 1.30 Å. From this lowest energy structure, the CO$_2$ molecule can rotate over the Pd$_3$ face to form a $\mu^3\eta^2$ geometry, which possesses approximate C_s symmetry, and a highly activated CO bond, $r_{CO} = 1.36$ Å. In transition state Fig. 5-VI, the activated CO bond breaks ($\nu_{imag} = 261$ cm^{-1}), but this barrier lies above zero energy at +0.28 eV. Structure Fig. 5-VII is very similar to the μ^2-O and μ^2-CO structure calculated by Kalita and Deka for the coadsorption of O$_2$ and CO on Pd$_4$.[75] Continuing the reaction path in order to dissociate the CO molecule is highly disfavoured, crossing a barrier of +3.42 eV in order to reach a minimum +3.30 eV higher in energy than the separated Pd$_4$ + CO$_2$ reactants.

3.6 Pt$_4$

Our structure search identified a singlet open butterfly structure ($\phi = 135°$) as the global minimum structure. In contrast, Sebetci predicted a distorted tetrahedron ground state, followed by a butterfly structure, though these differed by only 0.1 eV per atom in binding energy.[76] Grönbeck and Andreoni reversed this prediction for the neutral Pd$_4$ cluster, and additionally predicted a Y-shape cluster as being low in energy, further noting that the singlet and triplet states were quasi-degenerate.[77] The butterfly structure was also predicted by Singh *et al.*[78] and by Kawazoe and coworkers.[79] We employ our singlet butterfly as a fragment with CO$_2$.

Platinum is of long-standing interest and use as a catalyst. Of particular note, Mafuné and coworkers used DFT to show that small Pt$_n$ ($n = 4$–12) clusters could undergo oxygen transfer reactions with N$_2$O the but did not catalyse the oxidation of CO, instead co-adsorbing O + CO.[80] Mass spectra generated in the same joint experimental – computational study were unable to identify CO$_2$ desorption from the Pt$_n$ clusters. In a later work, Green *et al.* predicted a dissociative (O + CO) global minimum for the reaction of the anionic Pt$_4^-$ cluster, but infrared multiphoton dissociation (IR-MPD) showed that the CO$_2$ molecule remained intact.[35]
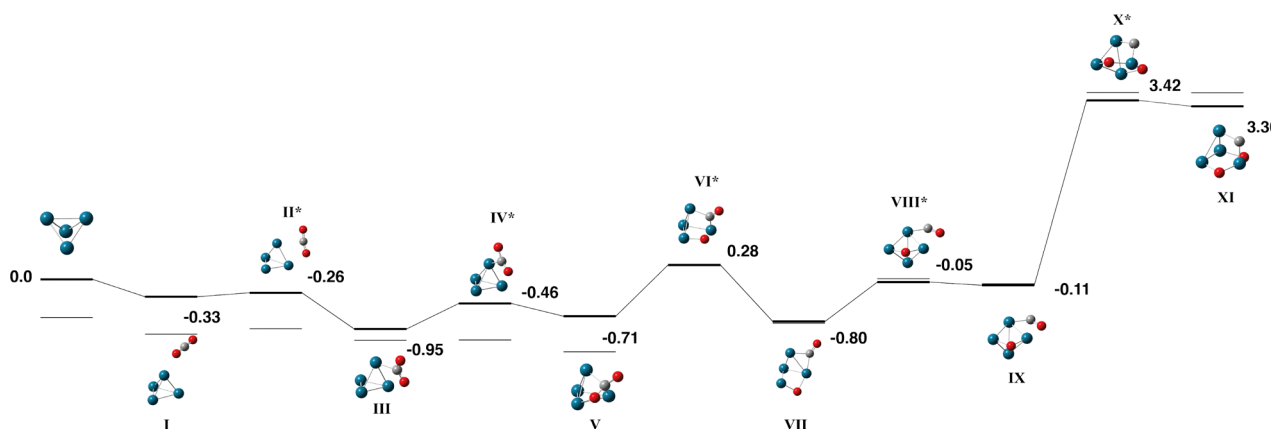

Fig. 5 Stationary points on the Pd$_4$ + CO$_2$ potential energy surface. The singlet multiplicity is shown in bold and the triplet multiplicity is shown with thin lines. Relative energies are given in eV. Metal atoms are shown in blue/green, oxygen atoms are shown in red and the carbon atom is shown in grey.

Fig. 6 Stationary points on the $Pt_4 + CO_2$ potential energy surface. The singlet multiplicity is shown in bold and the triplet–quintet multiplicities are shown with thin lines. Relative energies are given in eV. Metal atoms are shown in blue/green, oxygen atoms are shown in red and the carbon atom is shown in grey.
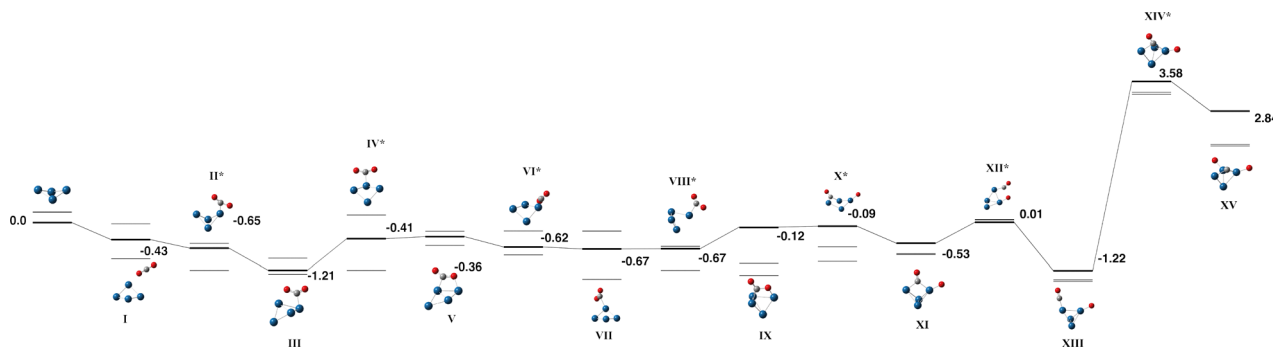
The calculated reaction path for neutral $Pt_4 + CO_2$ is shown in Fig. 6 with the corresponding data in Table S6. Green et al. noted that the anionic Pt_4^- cluster is a fluxional species,[35] and similar fluxionality is observed here for the neutral Pt_4 cluster, which contracts from an open butterfly structure, $\phi = 135°$ for Pt_4 to a tetrahedral structure, $\phi = 76°$ for the lowest energy structure Fig. 6-XIII. The key features on the reaction path are similar to those identified for the anionic cluster; after the capture species (Fig. 6-I), which is bound by −0.43 eV, a C-bound η^1 structure is formed (Fig. 6-III). The CO_2 molecule may be η^1-bound in this way to either an apex (Fig. 6-III) or spinal atom (Fig. 6-VII) of the Pt_4 butterfly, converting via an η^2 CO binding across the Pt–Pt bond (Fig. 6-V). From Fig. 6-IX, the CO_2 molecule could dissociate via either a opening/closing of the Pt_4 cluster (Fig. 6-X) or via stretching of the OC bond (Fig. 6-XII). The lowest energy Pt_4CO_2 structure has a μ^1-bound CO molecule with the dissociated oxygen atom μ^1 bound to an adjacent Pt atom. Searching for a pathway to dissociate the intact CO molecule identified a transition state +3.58 eV above

zero energy and a minimum +2.84 eV above zero energy, indicating that full dissociation of the CO_2 molecule to O + C + O is not thermodynamically feasible on the Pt_4 cluster.

3.7 Ag_4

Silver has an electronic configuration of $4d^{10}5s^1$, and we study the singlet–septet multiplicities. The global minimum Ag_4 structure is predicted to be a planar singlet rhombus structure of D_{2h} symmetry, in agreement with several previous calculations.[81–84] Attempts to converge a tetrahedral structure, similar to the Ag_4^{2+} structure calculated by Shimizu and coworkers, resulted in a stretched tetrahedron 0.95 eV higher in energy.[85] A recent study indicated that the diamond/rhombus structure of Ag_4 contributed strongly to the activation of O_2.[86]

The global minimum planar rhombus Ag_4 structure was used as the basis for the reaction path finding and the resulting $Ag_4 + CO_2$ reaction path is shown in Fig. 7 and Table S7. Only the singlet surface is shown as all other multiplicities were significantly above zero energy. CO_2 interacts only weakly with
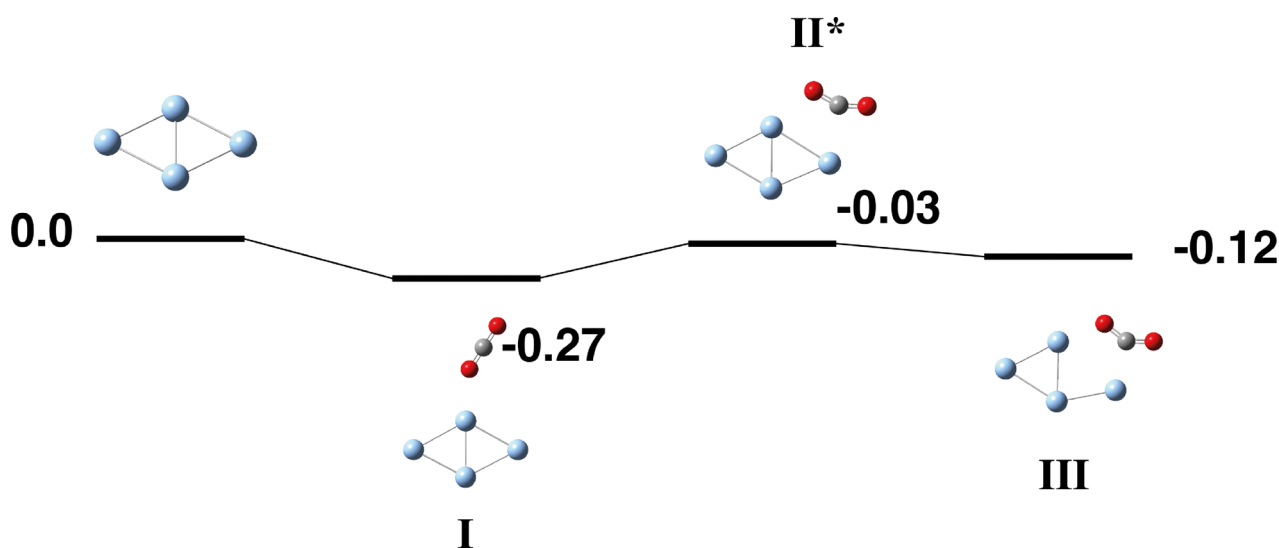

Fig. 7 Stationary points on the $Ag_4 + CO_2$ potential energy surface. The singlet multiplicity is shown with bold lines. Other multiplicities are high in energy and are not shown. Relative energies are given in eV. Metal atoms are shown in blue/green, oxygen atoms are shown in red and the carbon atom is shown in grey.

the Ag_4 cluster, the capture species (Fig. 7-I) has CO_2 μ^1-bound to a spinal Ag atom. The CO_2 molecule could then rotate in the Ag_4 plane and bend to form a $\mu^2\eta^2$ structure, but at the expense of the Ag–Ag bond, which is broken (3.79 Å *vs.* 2.76 Å). In Fig. 7-III, r(Ag–C) and r(Ag–O) are 2.23 and 2.24 Å respectively. No structures with CO_2 either partly (O + CO) or fully (O + C + O) dissociated were obtained.

3.8 Periodic trends

For each M_4 + CO_2 reaction path, several key species are identified, these are: (1) the capture species, which is always the first structure shown on each reaction path and represents the first (physisorption) interaction between CO_2 with the M_4 cluster, the CO_2 molecule is therefore still linear in the capture species. (2) The lowest energy species with associatively-bound CO_2, the CO_2 molecule is, by definition, intact, but may not be linear. This species represents an activated CO_2 molecule. If a stable activated CO_2 molecule could be thermodynamically or kinetically prevented from further activation → dissociation (to O + CO), the activated CO_2 might thus be available for reaction with *e.g.* H_2 to form formaldehyde. (3) The lowest energy structure with one CO bond broken, *i.e.* $M_4O\cdot CO$. (4) The lowest energy structure with the CO_2 fully dissociated to atoms. In the context of CO_2 activation, this would represent a catalyst poisoning process. The relative energies of these four geometric motifs are shown in Fig. 8.

The energy of the capture species is consistent across the periodic table, ranging from −0.23 eV (Mo_4) up to −0.48 eV for the square planar Ru_4 cluster. The consistency of this interaction is expected, given the definition of the capture species as the minimally interacting species and has been observed previously.[39] The relative energies of the associative (OCO), partly dissociated (O + CO) and fully dissociated (O + C + O) structures steadily increasing as one moves left to right across the periodic table, from Nb_4 to Ag_4. Note that no stuctures with dissociatively bound CO_2 were identified for Ag_4. The apparent 'slope' of energy increase, is mild for associative structures, moderate in the case of partly dissociated structures (O + CO) and strong for the fully dissociated structures. Fully dissociated structures are disfavoured (higher than zero energy) for Rh_4, Pd_4 and Pt_4. The energies for the third row Pt_4 cluster are similar, but slightly lower than the equivalent Pd_4CO_2 structures, suggesting that small clusters to the right of (and including) rhodium, would not fully dissociate CO_2.

The initial adsorption step is considered key to the activation of CO_2,[87] it is the first step where charge transfer from the cluster to the CO_2 molecule, typically *via* the electrophilic carbon atom occurs, weakening the C=O bonds, bending θ_{OCO} and thereby leading to a variety of stable intermediate structures.[87] We therefore consider the properties of the M_4CO_2 capture species for each reaction pathway: Table 1 shows the calculated vibrational frequencies of CO_2 in the capture species for each M_4 cluster. The two bending frequencies, now non-degenerate, are strongly red-shifted on interaction with the M_4 cluster, by ≈ 60 cm^{-1}, consistent with the CO_2 π_u antibonding orbitals receiving electron density from the
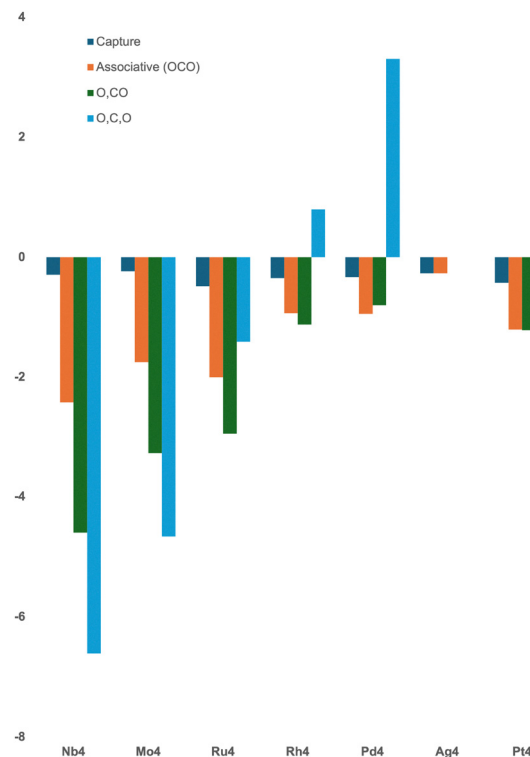

Fig. 8 Plot of the relative energies of capture, lowest energy associative (OCO), lowest energy partly dissociated (O,CO) and fully dissociative (O,C,O) structures of M_4 metal clusters in the singlet multiplicity.

cluster. Considering the first of the two formerly degenerate frequencies (the one with the larger redshift), there is an apparent, though approximate, correlation between the degree of redshift and the energy of the fully dissociative species, with clusters that possess a fully dissociated CO_2 below zero energy, regardless of whether this structure is the global minimum or not, show a redshift > 60 cm^{-1} (*viz.* Nb_4, Mo_4 and Ru_4). Clusters to the right of and including Rh_4 yield a smaller redshift.

Table 1 also shows the energy of the CO_2 π_u orbital and the ΔE, with respect to the calculated value for free CO_2 (−0.03280 a.u.). Clusters that thermodynamically dissociate CO_2 lower the energy of the π_u orbital by ≈ 1.2–1.5 eV, while clusters without a fully dissociated CO_2 below zero energy, lower the orbital energy by only ≈ 0.5–0.9 eV. Both of these correlations are indicative only, and provide no information on the relative stability of intermediate species (*e.g.* $M_4O\cdot CO$) but do act as a barometer for the thermodynamic stability (below zero energy) of the fully dissociative structure.

Table 1 shows the properties of the capture species for each reaction pathway, defined previously as the initial contact of CO_2 with the metal cluster. As this species possesses CO_2 physisorbed to the M_4 cluster, the interaction of the two species is minimal, and it is perhaps unsurprising that consideration of this species alone is insufficient to predict the eventual fate of CO_2. Table 2 shows the Hirshfeld charges on CO_2 molecule in the capture species and the first transition state for each of the reaction pathways. $q(CO_2)$ for the capture species is consistent

Table 1 CO_2 vibrational frequencies (ν_{CO_2}), key orbital energies and adsorption and interaction energies for M_4CO_2 capture species. Absolute energy of the CO_2 π_u orbital is -0.893 eV (-0.03280 a.u)

System	Bend 1	Bend 2	Symm stretch	Asym stretch	$E(M_{4,HOMO})$	$E(M_{4,LUMO})$	$E(\pi_u)$	$\Delta E(\pi_u)$	E_{ads}	E_{int}
			(cm^{-1})				(eV)			
CO_2	622	622	1283	2319			-0.893	0.0		
Nb_4	546	547	1256	2317	-4.237	-2.304	-2.304	-1.411	-0.291	-0.292
Mo_4	471	540	1251	2333	-3.920	-2.399	-2.399	-1.507	-0.237	-0.516
Ru_4	527	579	1268	2324	-4.905	-3.470	-2.140	-1.248	-0.481	0.514
Rh_4	572	587	1275	2322	-5.416	-3.000	-1.393	-0.501	-0.349	-0.351
Pd_4	581	585	1277	2322	-5.495	-4.245	-1.498	-0.605	-0.333	-0.341
Ag_4	599	606	1292	2331	-5.232	-3.130	-1.822	-0.930	-0.269	-0.269
Pt_4	567	588	1280	2330	-6.060	-4.227	-1.797	-0.904	-0.430	-0.433

Table 2 Hirshfeld charge on CO_2 in capture species and first transition state for M_4CO_2 reaction pathways

	Capture species	TS 1
System	$q(CO_2)$	$q(CO_2)$
Nb_4	0.098	-0.577
Mo_4	0.097	-0.488
Ru_4	0.125	-0.354
Rh_4	0.097	-0.299
Pd_4	0.080	-0.006
Ag_4	0.087	-0.151
Pt_4	0.114	-0.250

and positive (≈ 0.1) for all M_4 clusters, and clearly represents the initial donation of charge from the CO_2 molecule to the cluster. The charge transfer observed in the first transition state (*i.e.* the back-donation from the M_4 cluster to the CO_2 molecule upon chemisorption) is diagnostic, with the three species where full CO_2 dissociation is thermodynamically possible (*viz.* Nb_4, Mo_4 and Ru_4) having $q(CO_2) < -0.35e^-$. Clusters that do not dissociate either CO_2 bond, (Pd_4 and Ag_4) have low back-donation to CO_2, $< 0.2e^-$ and clusters that are likely to activate CO_2 without fully dissociating it, Rh_4, Pt_4, having intermediate $q(CO_2)$ values.

Fig. 9 shows the barrier heights (transition state energies) for the key transition states in each pathway. The chosen
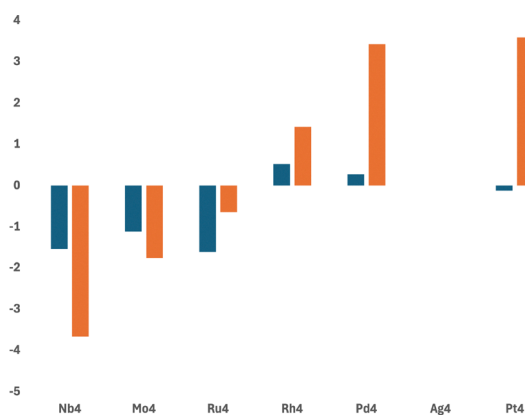

Fig. 9 Plot of the relative energies of barriers to dissociation of the first (blue) and second (orange) C⋯O bonds for M_4CO_2 reaction pathways on the singlet surface.

barriers correspond to each CO bond breaking. Accordingly, no barriers are plotted for Ag_4. Two trends can be clearly observed. Firstly, there is a clear left-right divide with all Nb_4–Ru_4 barriers being below zero energy, whereas Rh_4–Pd_4 barriers are above zero energy. The barrier to breaking the first CO bond on Pt_4 is slightly below zero energy at -0.12 eV, reflecting the softer surface presented by the 5d metal compared to its 4d counterpart. Secondly, the barriers to the first CO bond breaking are relatively consistent either side of the left-right divide defined by Ru/Rh, whereas the barrier to the second CO bond breaking rises when moving from left to right (Nb_4–Ag_4), suggesting that activated CO_2 or O + CO are likely outcomes of reaction on the Rh_4 and Pd_4 clusters.

The general trends in adsorption energies shown in Fig. 8 are consistent with other materials proposed for CO_2 adsorption. Peng and coworkers studied the adsorption of molecular CO_2 on M_2N MXenes, and found that end-on CO_2 binding had a consistent binding energy, of ≈ -0.25 eV, corresponding to a physisorbed geometry, but the adsorption energy of side-on CO_2 rose from -2.5 eV for Y_2N to -1.5 eV for Mo_2N, and MXenes to the right of Ru_2N bound CO_2 only weakly, ≈ -0.42 eV. Jurado *et al.* also studied a range of M_2X MXenes, finding similar binding energies and trends with CO_2 adsorption energies of -2.83, -1.73 and -1.34 eV for M = Zr, Nb and Mo respectively. In addition, they also noted the non-negligible role of the X atom, with carbides having lower adsorption energies than equivalent nitrides, and M_3N_2 MXenes having adsorption energies ≈ 1 eV greater than the equivalent M_2N species. A study on single-atom doped Ti_2CO_2 showed that CO_2 remains intact on these species, which is consistent with the CO_2 adsorption energy on Y-doped Ti_2CO_2 of -0.808 eV,[88] compared to ≈ 2 eV for the M_4 species that dissociate CO_2 in this work.

4 Conclusions

We have calculated reaction pathways for the reaction of CO_2 on a series of neutral M_4 transition metal clusters. Moving from left to right across the periodic table, the energies of the capture species remained relatively constant. The energies of the lowest energy M_4CO_2 species with CO_2 fully intact (associatively bound CO_2), lowest energy $M_4O\cdot CO$ species and $M_4O\cdot C\cdot O$ (fully dissociated CO_2) species all rose moving from Nb_4 to Ag_4, with the rate of increase $M_4O\cdot C\cdot O > M_4O\cdot CO > M_4CO_2$. Therefore it is

predicted that Nb_4 and Mo_4 will fully dissociate CO_2. Ru_4 may also fully dissociate CO_2, but would be more likely to only break the first CO bond, resulting in a $Ru_4O \cdot CO$ product. Rh_4, Pd_4 and Pt_4 are good candidates to observe an activated CO_2 molecule. The Ag_4 cluster interacts only weakly with CO_2. The energy of the CO_2 π_u orbital in the M_4CO_2 capture species and the related ν_{bend} was found to indicate those structures that dissociate CO_2 fully (Nb_4, Mo_4 and Ru_4) from those that do not, but did not distinguish between partly dissociated (O + CO) and fully intact CO_2, however the degree of charge transfer in the first transition state was found to indicate all three possible fates of CO_2.

Author contributions

SS, BAV, NA, MS: investigation, writing – original draft MAA: conceptualization of this study, methodology, writing – review and editing.

Conflicts of interest

There are no conflicts to declare.

Data availability

The data supporting this article have been included as part of the supplementary information (SI). Supplementary information: geometric parameters (pdf), structures (xyz) and energies, vibrational data (xlsx) for all pathways. See DOI: https://doi.org/10.1039/d5cp03419a.

Acknowledgements

Notes and references

1 G. A. Olah, G. K. S. Prakash and A. Goeppert, *J. Am. Chem. Soc.*, 2011, **133**, 12881–12898.

2 E. V. Kondratenko, G. Mul, J. Baltrusaitis, G. O. Larrazábal and J. Pérez-Ramírez, *Energy Environ. Sci.*, 2013, **6**, 3112–3135.

3 R. W. Dorner, D. R. Hardy, F. W. Williams and H. D. Willauer, *Energy Environ. Sci.*, 2010, **3**, 884–890.

4 A. G. Saputro, A. L. Maulana, F. D. Aprilyanti and H. K. Dipojono, *J. Eng. Technol. Sci.*, 2021, **53**, 210402.

5 V. K. Ocampo-Restrepo, L. G. Verga and J. L. F. Da Silva, *J. Phys. Chem. C*, 2021, **125**, 26296–26306.

6 X. Li, J. Yu, M. Jaroniec and X. Chen, *Chem. Rev.*, 2019, **119**, 3962–4179.

7 T. Sakakura, J.-C. Choi and H. Yasuda, *Chem. Rev.*, 2007, **107**, 2365–2387.

8 V. K. Ocampo-Restrepo, L. G. Verga and J. L. F. Da Silva, *J. Phys. Chem. C*, 2021, **125**, 26296–26306.

9 V. K. Ocampo-Restrepo, L. Zibordi-Besse and J. L. F. Da Silva, *J. Chem. Phys.*, 2019, **151**, 214301.

10 J. M. Weber, *Int. Rev. Phys. Chem.*, 2014, **33**, 489–519.

11 M. C. Thompson, J. Ramsay and J. M. Weber, *J. Phys. Chem. A*, 2017, **121**, 7534–7542.

12 C. Wu, M. Luo, Y. Zhao, S. Wang, A. Zavabeti, P. Xiao and G. K. Li, *Chem. Eng. J.*, 2023, **475**, 146411.

13 Q. Sun, S. Huang, Z. Li, D. Su and J. Sun, *J. Environ. Chem. Eng.*, 2023, **11**, 109065.

14 M. Zhang, D. Zhang, X. Jing, B. Xu and C. Duan, *Angew. Chem., Int. Ed.*, 2024, **63**, e202402755.

15 P. Du, G. Deng, Z. Li, J. Sun, L. Wang, Y. Yang, J. Wang, Y. Li, X. Xu, Y. Zhang, W. Liu, G. Liu, Z. Zou and Z. Li, *J. Mater. Sci. Technol.*, 2024, **189**, 203–210.

16 Y. Wang, Y. S. Chan, R. Zhang and B. Yan, *Chem. Eng. J.*, 2024, **481**, 148360.

17 O. Hurtado-Aular, R. M. Ferullo and P. G. Belelli, *Comput. Mater. Sci.*, 2024, **233**, 112741.

18 Y. Shao, S. Zhang, X. Ou, F. Zeng, R. Cai, X. Fan and H. Chen, *Chem. Eng. J.*, 2025, **518**, 164589.

19 D. Y. Shin, J. H. Jo, J.-Y. Lee and D.-H. Lim, *Comput. Theor. Chem.*, 2016, **1083**, 31–37.

20 H. Sugiyama, M. Miyazaki, M. Sasase, M. Kitano and H. Hosono, *J. Am. Chem. Soc.*, 2023, **145**, 9410–9416.

21 V. Muman, A. Tennyson-Davies, O. Allegret and M. A. Addicoat, *Phys. Chem. Chem. Phys.*, 2024, **26**, 2218–2227.

22 M. A. Addicoat, K. F. Lim and G. F. Metha, *J. Chem. Phys.*, 2012, **137**, 034301.

23 A. Fielicke, *Chem. Soc. Rev.*, 2023, **52**, 3778–3841.

24 A. Yamada, K. Miyajima and F. Mafune, *Phys. Chem. Chem. Phys.*, 2012, **14**, 4188–4195.

25 D. Harding, M. S. Ford, T. R. Walsh and S. R. Mackenzie, *Phys. Chem. Chem. Phys.*, 2007, **9**, 2130–2136.

26 S. Nayak, B. Rao, S. Khanna and P. Jena, *Chem. Phys. Lett.*, 1996, **259**, 588–592.

27 G. Kwon, G. A. Ferguson, C. J. Heard, E. C. Tyo, C. Yin, J. DeBartolo, S. Seifert, R. E. Winans, A. J. Kropf, J. Greeley, R. L. Johnston, L. A. Curtiss, M. J. Pellin and S. Vajda, *ACS Nano*, 2013, **7**, 5808–5817.

28 R. K. Raju, P. Rodriguez and E. N. Brothers, *Phys. Chem. Chem. Phys.*, 2023, **25**, 11630–11652.

29 K. Mori, J. Matsuo, Y. Kondo, H. Hata and H. Yamashita, *ACS Appl. Energy Mater.*, 2021, **4**, 11634–11642.

30 S. H. Pulumati, D. K. Sannes, C. R. Jabbour, L. D. B. Mandemaker, B. M. Weckhuysen, U. Olsbye, A. Nova and E. Skulason, *ACS Catal.*, 2023, **14**, 382–394.

31 M. N. Collacique, V. K. Ocampo-Restrepo and J. L. F. Da Silva, *J. Chem. Phys.*, 2022, **156**, 124106.

32 D. Guo, J. Liu, X. Zhao, X. Yang and X. Chen, *Sep. Purif. Technol.*, 2023, **313**, 123462.

33 J. Li, P. Gonzalez-Navarrete, M. Schlangen and H. Schwarz, *Chem. – Eur. J.*, 2015, **21**, 7780–7789.

34 M. A. Nolen, S. A. Tacey, S. Kwon and C. A. Farberow, *Appl. Surf. Sci.*, 2023, **637**, 157873.

35 A. E. Green, J. Justen, W. Schöllkopf, A. S. Gentleman, A. Fielicke and S. R. Mackenzie, *Angew. Chem., Int. Ed.*, 2018, **57**, 14822–14826.

36 U. Mondal and P. Ghosh, *Catal. Today*, 2021, **370**, 93–103.

37 M. A. Addicoat and G. F. Metha, *J. Comput. Chem.*, 2009, **30**, 57–64.

38 M. A. Addicoat, S. Fukuoka, A. J. Page and S. Irle, *J. Comput. Chem.*, 2013, **34**, 2591–2600.

39 M. A. Addicoat, M. A. Buntine, B. Yates and G. F. Metha, *J. Comput. Chem.*, 2008, **29**, 1497–1506.

40 A. D. Becke, *J. Chem. Phys.*, 1993, **98**, 5648–5652.

41 P. J. Hay and W. R. Wadt, *J. Chem. Phys.*, 1985, **82**, 270–283.

42 W. R. Wadt and P. J. Hay, *J. Chem. Phys.*, 1985, **82**, 284–298.

43 P. J. Hay and W. R. Wadt, *J. Chem. Phys.*, 1985, **82**, 299–310.

44 M. A. Addicoat, K. F. Lim and G. F. Metha, *J. Chem. Phys.*, 2012, **137**, 034301.

45 J. Tao, J. P. Perdew, V. N. Staroverov and G. E. Scuseria, *Phys. Rev. Lett.*, 2003, **91**, 146401.

46 F. Weigend and R. Ahlrichs, *Phys. Chem. Chem. Phys.*, 2005, **7**, 3297–3305.

47 F. Weigend, *Phys. Chem. Chem. Phys.*, 2006, **8**, 1057–1065.

48 S. Grimme, S. Ehrlich and L. Goerigk, *J. Comput. Chem.*, 2011, **32**, 1456–1465.

49 E. M. Cunningham, A. S. Gentleman, P. W. Beardsmore and S. R. Mackenzie, *Phys. Chem. Chem. Phys.*, 2019, **21**, 13959–13967.

50 G. Meizyte, A. E. Green, A. S. Gentleman, S. Schaller, W. Schöllkopf, A. Fielicke and S. R. Mackenzie, *Phys. Chem. Chem. Phys.*, 2020, **22**, 18606–18613.

51 M. J. Frisch, G. W. Trucks, H. B. Schlegel, G. E. Scuseria, M. A. Robb, J. R. Cheeseman, G. Scalmani, V. Barone, G. A. Petersson, H. Nakatsuji, X. Li, M. Caricato, A. V. Marenich, J. Bloino, B. G. Janesko, R. Gomperts, B. Mennucci, H. P. Hratchian, J. V. Ortiz, A. F. Izmaylov, J. L. Sonnenberg, D. Williams-Young, F. Ding, F. Lipparini, F. Egidi, J. Goings, B. Peng, A. Petrone, T. Henderson, D. Ranasinghe, V. G. Zakrzewski, J. Gao, N. Rega, G. Zheng, W. Liang, M. Hada, M. Ehara, K. Toyota, R. Fukuda, J. Hasegawa, M. Ishida, T. Nakajima, Y. Honda, O. Kitao, H. Nakai, T. Vreven, K. Throssell, J. A. Montgomery, Jr., J. E. Peralta, F. Ogliaro, M. J. Bearpark, J. J. Heyd, E. N. Brothers, K. N. Kudin, V. N. Staroverov, T. A. Keith, R. Kobayashi, J. Normand, K. Raghavachari, A. P. Rendell, J. C. Burant, S. S. Iyengar, J. Tomasi, M. Cossi, J. M. Millam, M. Klene, C. Adamo, R. Cammi, J. W. Ochterski, R. L. Martin, K. Morokuma, O. Farkas, J. B. Foresman and D. J. Fox, *Gaussian~16 Revision B.01*, Gaussian Inc., Wallingford CT, 2016.

52 X. X. Jin, J. G. Du, G. Jiang, X. Luo and X. W. Wang, *Eur. Phys. J. D*, 2011, **64**, 323–329.

53 P. V. Nhat, V. T. Ngan and M. T. Nguyen, *J. Phys. Chem. C*, 2010, **114**, 13210–13218.

54 P. Calaminici and R. Mejia-Olvera, *J. Phys. Chem. C*, 2011, **115**, 11891–11897.

55 X. Wang, M. Lin and Q. Zhang, *Acta Chim. Sin.*, 2004, **62**, 1689–1694.

56 C. V. S. Costa, L. d S. Barbosa, R. Gargano and D. L. Azevedo, *J. Mol. Mod.*, 2024, **30**, 406.

57 D. Majumdar and K. Balasubramanian, *J. Chem. Phys.*, 2004, **121**, 4014–4032.

58 Y. Wei, V. Veryazov and L. Kantorovich, *APL Mater.*, 2024, **12**, 031127.

59 S. Liebing, C. Martin, K. Trepte and J. Kortus, *Phys. Rev. B: Condens. Matter Mater. Phys.*, 2015, **91**, 155421.

60 Y.-H. Yin and J. Chen, *Comput. Theor. Chem.*, 2022, **1212**, 113720.

61 A. Sumer and J. Jellinek, *J. Chem. Phys.*, 2022, **157**, 034301.

62 R. Pis Diez, *Int. J. Quantum Chem.*, 2000, **76**, 105–112.

63 G.-X. Ge, H.-X. Yan, Q. Jing and Y.-H. Luo, *J. Cluster Sci.*, 2011, **22**, 473–489.

64 Y.-C. Bae, H. Osanai, V. Kumar and Y. Kawazoe, *Mater. Trans.*, 2005, **46**, 159–162.

65 F. Aguilera-Granja, L. C. Balbás and A. Vega, *J. Phys. Chem. A*, 2009, **113**, 13483–13491.

66 B. V. Reddy, S. K. Nayak, S. N. Khanna, B. K. Rao and P. Jena, *Phys. Rev. B: Condens. Matter Mater. Phys.*, 1999, **59**, 5214–5222.

67 T. Futschek, M. Marsman and J. Hafner, *J. Phys.: Condens. Matter*, 2005, **17**, 5927.

68 C.-H. Chien, E. Blaisten-Barojas and M. R. Pederson, *Phys. Rev. A: At., Mol., Opt. Phys.*, 1998, **58**, 2196–2202.

69 S. K. Nayak, S. E. Weber, P. Jena, K. Wildberger, R. Zeller, P. H. Dederichs, V. S. Stepanyuk and W. Hergert, *Phys. Rev. B: Condens. Matter Mater. Phys.*, 1997, **56**, 8849–8854.

70 Y. Jinlong, F. Toigo and W. Kelin, *Phys. Rev. B: Condens. Matter Mater. Phys.*, 1994, **50**, 7915–7924.

71 V. Kumar and Y. Kawazoe, *Phys. Rev. B: Condens. Matter Mater. Phys.*, 2002, **66**, 144413.

72 R. L. Camacho-Mendoza and J. Cruz-Borbolla, *Chem. Phys. Lett.*, 2020, **755**, 137794.

73 X. Tang, W. Zeng, H. Duan, S. Chen and X. Lian, *React. Kinet., Mech. Catal.*, 2023, **136**, 1933–1943.

74 P. Dutta, N. Biswakarma, D. Dowerah, S. Neog, A. Phonglo, P. J. Sarma, N. K. Gour and R. C. Deka, *J. Phys. Chem. C*, 2024, **128**, 21263–21279.

75 B. Kalita and R. C. Deka, *J. Am. Chem. Soc.*, 2009, **131**, 13252–13254.

76 A. Sebetci, *J. Chem. Phys.*, 2006, **331**, 9–18.

77 H. Grönbeck and W. Andreoni, *Chem. Phys.*, 2000, **262**, 1–14.

78 N. B. Singh and U. Sarkar, *J. Mol. Mod.*, 2014, **20**, 2537.

79 V. Kumar and Y. Kawazoe, *Phys. Rev. B: Condens. Matter Mater. Phys.*, 2008, **77**, 205418.

80 H. Yamamoto, K. Miyajima, T. Yasuike and F. Mafuné, *J. Phys. Chem. A*, 2013, **117**, 12175–12183.

81 N. Hartmann, R. Mitric, B. Stanca and V. Bonacic-Koutecky, *Eur. Phys. J. D*, 2001, **16**, 151–155.

82 V. Bonačić-Koutecky, L. Češpiva, P. Fantucci and J. Koutecky, *J. Chem. Phys.*, 1993, **98**, 7981–7994.

83 Y. Wang and X. G. Gong, *Eur. Phys. J. D*, 2005, **34**, 19–22.

84 R. Fournier, *J. Chem. Phys.*, 2001, **115**, 2165–2177.

85 S. Yasumura, T. Kato, T. Toyao, Z. Maeno and K.-I. Shimizu, *Phys. Chem. Chem. Phys.*, 2023, **25**, 8524–8531.

86 W. Wang, X. Liu and J. Pérez-Ros, *J. Phys. Chem. A*, 2021, **125**, 5670–5680.

87 M. N. Collacique, V. K. Ocampo-Restrepo and J. L. F. Da Silva, *J. Chem. Phys.*, 2022, **156**, 124106.

88 Y.-X. Yu, *J. Colloid Interface Sci.*, 2025, **695**, 137799.